Engineering Multisite Metal-Organic Cages with Metal Acyl Nodes for Specific Recognition and Deep Purification of Radioactive Strontium(II)

Wei Jin[+], [a, b] Qun-yan Wu[+], [b] Yan Lou, [b] Zhi-wei Huang, [b] Feng Liu, [b] Bo-wen Hu, [b] Ji-pan Yu, [b] Kong-qiu Hu, [b] Li-yong Yuan, [b] Wei-qun Shi*, [a, b] and Lei Mei*[b]

[a] College of Nuclear Science and Technology, Harbin Engineering University, Harbin 150001, China

[b] Laboratory of Nuclear Energy Chemistry, Institute of High Energy Physics, Chinese Academy of Sciences, Beijing 100049, China.

[+] These authors contributed equally to this work.

* E-mail: shiwq@ihep.ac.cn; meil@ihep.ac.cn

Abstract: Tailored design of organic linkers or metal nodes can implant desirable binding sites in metal-organic cages (MOCs) and greatly expand the type of guest they can encapsulate. In this work, we propose a feasible method of engineering acyl-type metal nodes to endow MOCs with selective recognition ability towards metal ions without compromising structural robustness of MOCs. A novel MOC with a uranyl-sealed calix[4]resorcinarene (C[4]R)-based multisite cavity, namely **UOC**, is synthesized as a prototype compound. In **UOC**, peroxide-bridged dimeric uranyl units on both sides of the coordination cage offer abundant coordination-available oxygen sites, creating a cryptand-like cavity that enables high-efficient recognition and encapsulation of Sr^{2+} ion due to precise size-matching effect. Bonding analysis of the resultant Sr@**UOC** suggest that, although electrostatic interaction predominates in host-guest interactions between **UOC** and Sr^{2+}, there is significant degree of overlapping between Sr 4d and O 2p orbitals, thus conforming the origin of high binding strength of **UOC** for Sr^{2+}. Meanwhile, hydrophobic binding cavities at both ends of **UOC** allow it to further encapsulate organic guests, thus facilitating co-inclusion of two different kinds of guest species in **UOC** for the first time. Inspired by the strong binding affinity of **UOC** to Sr^{2+}, it is employed as absorbents to capture Sr^{2+} ion of low concentrations in aqueous solution. A removal efficiency of 99.9% could be achieved for Sr^{2+} ions at the initial concentration as low as 0.01 mM, with a record distribution coefficient (K_d) as high as 1.36×10^7 mL/g, demonstrating its huge potential for deep purification of trace amount of radioactive $^{90}Sr^{2+}$.

INTRODUCTION

Biological proteins, that consist of a group of domains gathered together through supramolecular interactions are often involved in massive molecular recognition events to underpin important processes essential for life.[1-3] Inspired by nature, exploration of artificial supramolecular architectures with the capability to bind guest molecules have garnered much attention for several decades. Among typical supramolecular systems, metal-organic cages (MOCs) are a class of discrete metal-containing architectures that are constructed by coordination-driven self-assembly between metal nodes and organic structs.[4-11] The modularity of metal-ligand coordination, in combination of the availability of customizing organic ligand as desired,[4, 8, 9, 12, 13] renders the successful establishment of a portfolio of metallo-supramolecular architectures with tailored well-defined cavities that can accommodate different kinds of guest molecules.[14-18] Since the cavities of MOCs might be tailored to meet stringent requirements on the guests' geometry and binding preferences, high selectivity in guest binding are expected in such cavities, thereby enabling the achievement of specific separation of the target guests.[14, 19-21] However, there is still enormous synthetic challenge in the rational design and regulation of MOCs on demand, particularly for those with increased dimensions and complexity designed for efficient recognition of specific kinds of guest species in applications.

Benefitting from the inherent large-size cavities in MOCs, excellent encapsulation ability for organic molecules of different sizes is achieved through weak interactions of varying strengths (such as hydrogen bonding, halogen bonds, pi-pi stacking, ionic dipole interactions or hydrophobic interactions) between host cages and encapsulated species.[22] Besides, inorganic anions are another kind of important guests for MOCs, which can be selectively trapped in the cavities of MOCs mainly through electrostatic interactions and hydrogen bonds.[16, 21, 23-26] Since the fact that a majority of MOCs are assembled from neutral ligands and cationic metal centers, counter anions are inherently associated with the resultant positively charged supramolecular skeletons, and even serve as synthetic templates for MOCs in many case. In contrast, few research is devoted to the in-cage recognition of metal cations by MOCs. Recently, endeavors

by supramolecular chemists to modify the charged properties of coordination cages facilitate the in-situ encapsulation of hydrated cations under specific solvents and temperatures.[27, 28] Nevertheless, the predominant mechanisms for the hydrated metal ion encapsulation still rely on weak hydrogen bonding and electrostatic interactions resembling the case observed for anion recognition. These weak interactions result in poor encapsulation yield (only ~70% in pure water) to targeted metal ions, and solvent environments for binding of hydrated metal ions are quite distinctive from actual conditions of wastewater treatment,[29, 30] hindering the practical application of this method for metal ion capture in contaminated wastewater. Therefore, it is highly desirable to develop applicable MOCs for selective recognition of target metal ions by metal-ligand coordination.

The most critical issue for selective binding of metal ions by MOCs is to impart additional coordination sites into MOCs, either on organic linkers or on metal centers, without affecting the stability of well-defined MOCs themselves. Learning from post-synthetic modification of MOF materials based on a multifunctional ligand-based method,[31] functionalization of organic linkers with two or more orthogonal coordination sites for recognize different kinds of metal centers are required, so that coordination sites for second metal ion capture is preserved during coordination assembly process of MOCs (**Figure 1a**). However, it is difficult to achieve such a modification of MOCs due to high susceptibility of MOCs' synthesis to varying molecular sizes, configuration and functionality of organic ligands,[32] with only limited success in a very small number of robust MOCs.[33, 34] Alternatively, metal nodes in MOCs have great potential to provide efficient binding sites for guest species. For example, guest molecules or anions can be trapped on MOCs through occupation of unsaturated coordination sites of metal nodes by their functional groups, enabling effective implantation of these guest species (**Figure 1a**).[24-26, 35-38] Inspired by these MOCs with additional functionality in metal nodes, it can be envisioned that, by introducing metal ions with additional binding sites (such as metal acyl, e.g. uranyl or vanadyl) as the nodes of MOCs, the axial oxygen atoms on the metal acyl nodes, probably together with other adjacent functional groups, can be further utilized for capture second metal ions by metal-ligand coordination (**Figure 1b**). In fact, the coordination ability of axial oxygen

atoms of uranyl ion has been intensively demonstrated in the numerous uranyl compounds with typical cation-cation interactions (CCIs).[39-43] Therefore, the incorporation of uranyl nodes can be taken as a feasible method to introduce recognition sites for second metal ions into MOCs, and efficient recognition of targeted metal ions by MOCs is expected based on metal node engineering.

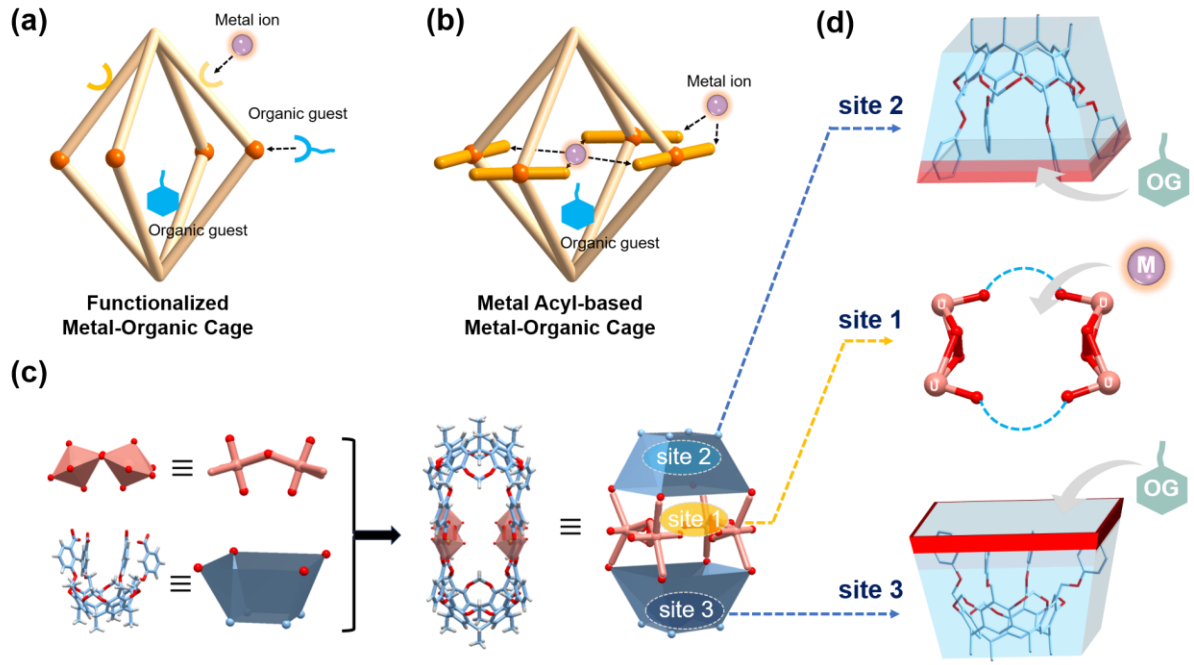

Figure 1. Design and preparation of multisite metal-organic cages through metal node engineering: (a) a traditional metal-organic cage functionalized with coordination unsaturated metal nodes and organic linkers for recognition of organic molecules and secondary metal ions, respectively; (b) a metal acyl-based metal-organic cage using residual coordination capacity of the axial oxygen atoms on the metal nodes as recognition sites for second metal ions; (c) coordination driven assembly of **UOC** from calix[4]resorcinarene tetracarboxylate linkers and in-situ formed peroxide-bridged dimeric uranyl nodes (d) with three possible recognition sites for both metal ions and organic guests. Color codes: purple balls labelled as 'M' refer to a metal ion, and light green hexagons with tails labelled as 'OG' refer to organic molecules.

Herein, by employing uranyl as a functional module for assembling with calix[4]resorcinarene tetracarboxylate ligand (abbreviated as C[4]R), a novel uranyl-based MOC compound with peroxo-bridged dimeric uranyl nodes, $[(UO_2)_4(O_2)_2(C[4]R)_2 \cdot 2DMF]$ (namely **UOC**), was synthesized solvothermally (**Figure 1c**). As expected, an oxygen-rich coordination site featured with a precisely defined cryptand-like cavity size is present in **UOC**, which is created by two sets of dimeric uranyl nodes at both sides of UOC that are forced to

be spatially close to each other by C[4]R macrocycle with inherent constraints in molecular configuration (**Figure 1d**). Sr^{2+} ions are well encapsulated within this cryptand-like cavity of **UOC**, which was confirmed through a combination of characterization techniques including nuclear magnetic resonance spectroscopy (^{1}H-NMR), mass spectrometer (HR-FTMS), infrared spectroscopy (FT-IR), energy dispersive X-ray spectroscopy (EDX) and single-crystal X-ray diffraction analysis (SCXRD). Meanwhile, the electron-rich cavity of C[4]R, acting as two additional interior hydrophobic recognition sites located at both ends of **UOC**, enables further encapsulation of organic guests, allowing for multi-guest encapsulation of both organic and inorganic subcomponents within a single cage. Benefiting from this coordination-based affinity to Sr^{2+}, **UOC** can achieve highly selective removal of ultra-low concentrations of radioactive Sr^{2+} ions, even in competitive natural water systems, which is favorable to deep purification of trace levels of radioactive contaminants.

RESULTS AND DISCUSSION

Synthesis and Characterization of UOC.

Yellow prism crystals of **UOC** (**Figure S4**) were obtained by heating a mixture of C[4]R and $UO_2(NO_3)_2{\cdot}6H_2O$ dissolved in a DMF/H_2O (3:1 v/v) mixed solvent at 100°C for 72 hours. X-ray crystallographic analysis revealed that **UOC** crystallizes in the orthorhombic space group $Cmc2_1$ (**Table S1**). Beside a pair of DMF solvent molecules, each cage unit in **UOC** contains two C[4]R ligands and two sets of peroxo-bridging dimeric uranyl units that both serve as tetrapodal metallo-constructs to form a twisted anionic capsule $[(UO_2)_4(O_2)_2(C[4]R)_2]^{4-}$ (**Figure 1c** and **Figure S5**). The O-O distance of peroxo group is 1.537(9) Å, which is consistent with those reported in other uranyl peroxide compounds and rule out the possibility of misidentification of hydroxyl groups.[44, 45] Although photoinduced reduction of oxygen in air in the presence of uranyl ion to generate peroxide has been previously reported in several studies,[46-49] what is found here should be a type of thermally-induced oxygen reduction,[50] where the reductive capability of organic ligand C[4]R towards oxygen atmosphere at elevated temperatures and its coordination stabilization effect on dimeric uranyl units bridged by in-situ formed peroxide groups (**Figure 2a**) is crucial to final formation of **UOC**. In addition to (μ_2-

η^2, η^2)-coordinated peroxo group, each eight-fold coordinated uranyl is also coordinated to another two η^2-carboxyl groups (**Figure 2b**) with slightly longer U-O(carboxyl) bonds (2.404(7) Å-2.539(7) Å) than those of U-O(peroxo) bonds (2.317(6) Å-2.370(6) Å) (**Table S2**), thus taking a hexagonal bipyramid geometry. Since the two uranyl centers are bridged by peroxo group to give dimeric unit with a U1-[O_2]-U2 dihedral angle is 140.8°, the equatorial planes of two uranyl-based hexagonal bipyramids are not is coplanar (**Figure 2c**). Correspondingly, the tetratopic C[4]R ligand adopts a mirror-symmetrical geometric conformation with two equivalent pairs of carboxylate groups, each of which coordinates to a dimeric uranyl-peroxo unit through different uranyl centers from both sides.

The most intriguing feature of **UOC** is its capsule-shape topologic structure with an elongated cavity. A similar uranyl-peroxo based MOC structure was also established from ditopic macrocyclic calix[4]pyrrole by Sessler et al (**Figure S6a-b**, referred to as cage-2 named by the authors).[49] Although the internal oxygen atoms oriented towards the center of the cavity in both uranyl-organic capsules are highly pre-organized, the two sets of peroxo-bridging dimeric uranyl units in **UOC**is much closer compared to that found in cage-2 (the distance between peroxo groups: 5.28(1) Å in **UOC** vs 6.40(1) Å in cage-2, see **Figure S6c-f**). The difference between **UOC** and cage-2 should be attributed to the utilization of a tetrapodal C[4]R ligand with relatively high rigidity, which 'pull' the two peroxo-bridging dimeric uranyl units to be spatially close to each other. Meanwhile, the U-[O_2]-U dihedral angle (140.8° in **UOC** vs 158.0° in cage-2) and U-U distances for each dimeric uranyl unit (4.168(1) Å in **UOC** vs 4.309(1) Å in cage-2) is also affected due to the restriction effect from macrocyclic C[4]R.[51] Consequently, axial oxygen atoms from uranyl centers, together with both the O-O bonds on the sides closer to the center of the cavity form a potential spherical recognition site for second metal ions. In contrast, cage-2 exhibits a longer U-U distance and a larger dihedral angle, with the oxygen atoms in its rectangular space far removed from the center of the cavity. Compared to cage-2, each macrocyclic C[4]R ligand at both ends of **UOC** also provide another hydrophobic cavity within the interior space of C[4]R itself. Consequently, the capsule structure in **UOC** comprises two kinds of potential recognition sites (**Figure 2d**): the first kind

is an oxygen-rich cryptand-like cavity in the middle of **UOC** in sizes of 5.28(1) Å and 5.25(1) Å (defined by the distance between two peroxide groups and that between two uranium centers along another direction), formed by the uranyl peroxide units, and the other kind is two open hydrophobic cavities surrounded by organic aromatic rings at both ends of **UOC** with the open sizes of 8.07(1) Å and 9.36(2) Å (defined by a pair of opposite bridging methylene groups), provided by C[4]R ligands.

The lattice stacking pattern of **UOC** in three-dimension crystal lattice shows the capsule units are all arranged in a staggered way (**Figure S7**), which helps to maintain the supramolecular framework unchanged in the ambient atmosphere (**Figure S8**). After dispersed in DMF solvents, Fourier transform high resolution mass spectrometry (FT-MS) of **UOC** reveals that **UOC** retains the integrity of the capsule structure in solution as dimers of C[4]R, with a triply charged negative ion peak observed at m/z = 1174.2551 (**Figure S9**), corresponding to the chemical composition $[C_{136}H_{105}O_{52}U_4]^{3-}$ of **UOC** after binding with a hydrogen proton. NMR spectroscopy (see the discussion in the following section) and other characterization results (**Figure S10-S12**) also prove the presence of uranyl and its coordination with C[4]R ligand in MOC. For instance, **UOC** dissolved in DMF exhibits several broad absorption peaks within the range of 420~460 nm in UV-visible region corresponding to the absorption band of uranyl center coordinated to carboxylate groups from C[4]R (**Figure S11**).

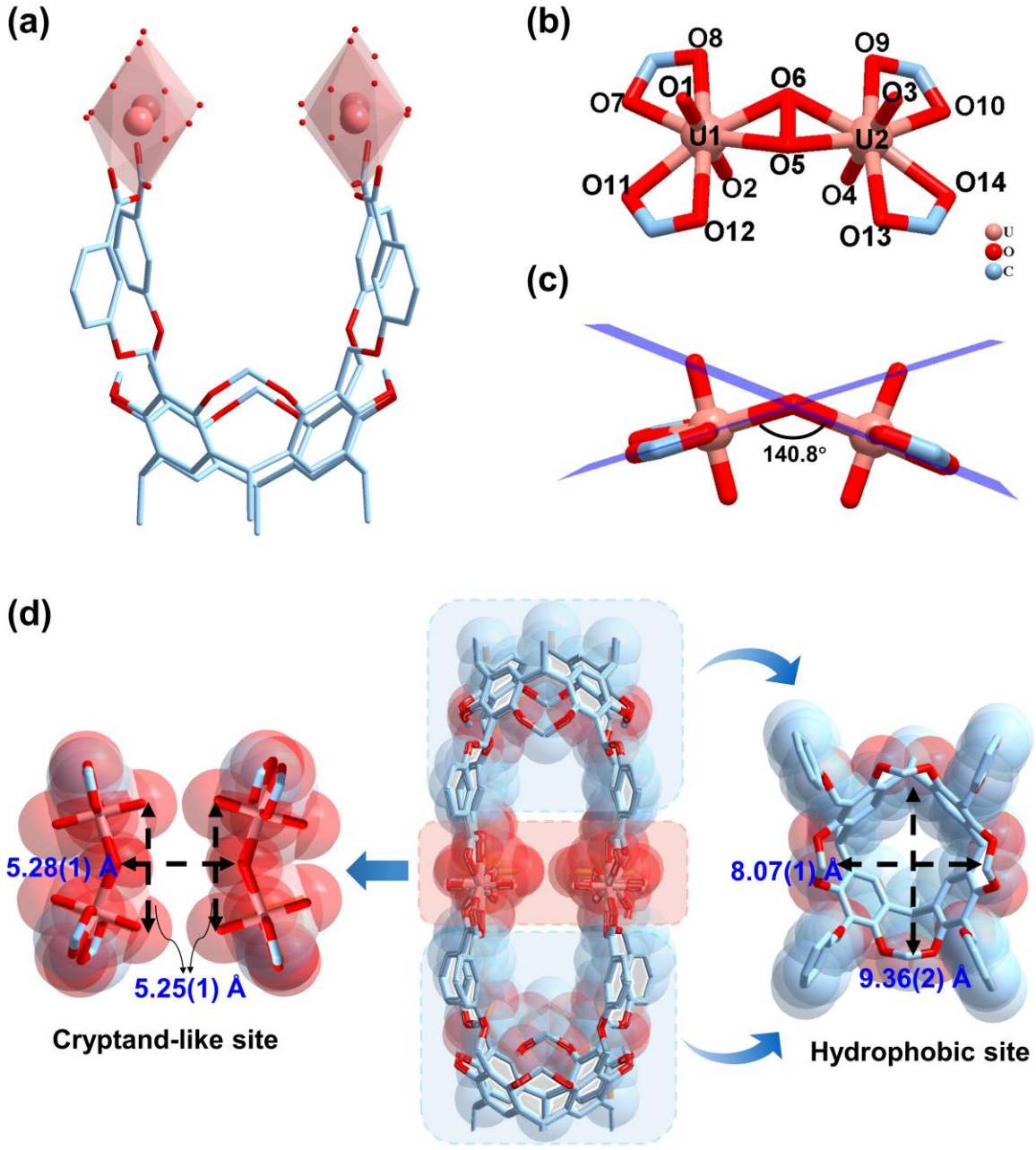

Figure 2. Crystal structure of **UOC** and potential supramolecular recognition sites in its internal cavity: (a) coordination of tetratopic C[4]R with dimeric uranyl units bridged by in-situ formed peroxide groups through two equivalent pairs of carboxylate groups, of which each binds to dimeric uranyl through different uranyl centers from both sides; (b, c) uranyl coordination spheres of the peroxo-bridged dimeric uranyl unit with a U-[O_2]-U dihedral angle of 140.8°; (d) two kinds of recognition sites found in capsule-shape **UOC** that include an oxygen-rich cryptand-like cavity in the middle of UOC in sizes of 5.28(1) Å and 5.25(1) Å and two open hydrophobic cavities surrounded by organic aromatic rings at both ends of UOC with the open sizes of 8.07(1) Å and 9.36(2) Å.

Sr^{2+} Ion Recognition and In-cage Encapsulation.

The well-defined pocket in **UOC**, which is formed by a pair of peroxo-bridging dimeric uranyl units that are spatially close to each other, is like a cryptand or crown ether in shape. Inspired by the selective recognition capabilities of traditional macrocyclic crown ethers towards various metal ions, i.e. strontium(II),[52-54] indium(III),[55-57] plutonium(V),[58] and et al, the internal functional groups may render UOC to behave as a metal receptor for the recognition of metal ions by providing an appropriate coordination environment.

Considering the cavity size of the cryptand-like pocket, Sr^{2+} ion, a typical alkaline earth metal ion was chosen as a representative to preliminarily verify the encapsulation capabilities of **UOC** for metal cations. The interaction between **UOC** and Sr^{2+} ion was first investigated by ^{1}H-NMR spectroscopy conducted in N, N'-dimethylformamide-d_7 (DMF-d_7) (**Figure 3a**). It can be seen that, protons adjacent to the carboxylate groups in **UOC** are deshielded due to uranyl coordination, leading to downfield shifts in proton signals at various positions (H_a, H_b, H_c, H_d) on the benzoic acid units. Splitting and downfield shifts were also observed in the methylene (H_f) signals of the benzoic acid side chains and the methylene (H_g) signals of the C[4]R skeleton. These shifts are attributed to the distorted molecular conformation following coordination assembly, resulting in the magnetic inequivalence of hydrogens on each methylene group. Upon loading Sr^{2+} ions in **UOC**, a noticeable high-field shift of 0.10 ppm is observed in the methylene proton signals on the terminal rings of the Sr@**UOC** skeleton. Furthermore, the signals of the methylene protons on the flexible side chains of Sr@**UOC** exhibit a change from a quartet mode to a doublet one. This reduction in peak splitting indicates there might be an increase in the cage's symmetry.[59] After immersing UOC crystals in a Sr^{2+} ion aqueous solution for 12 hours and subsequent separation, the solid phase was dissolved in DMF-d_7 for NMR spectroscopic analysis. The observed changes align with those in the liquid-phase Sr@**UOC**, providing crucial insights into the subsequent Sr^{2+} separation process.

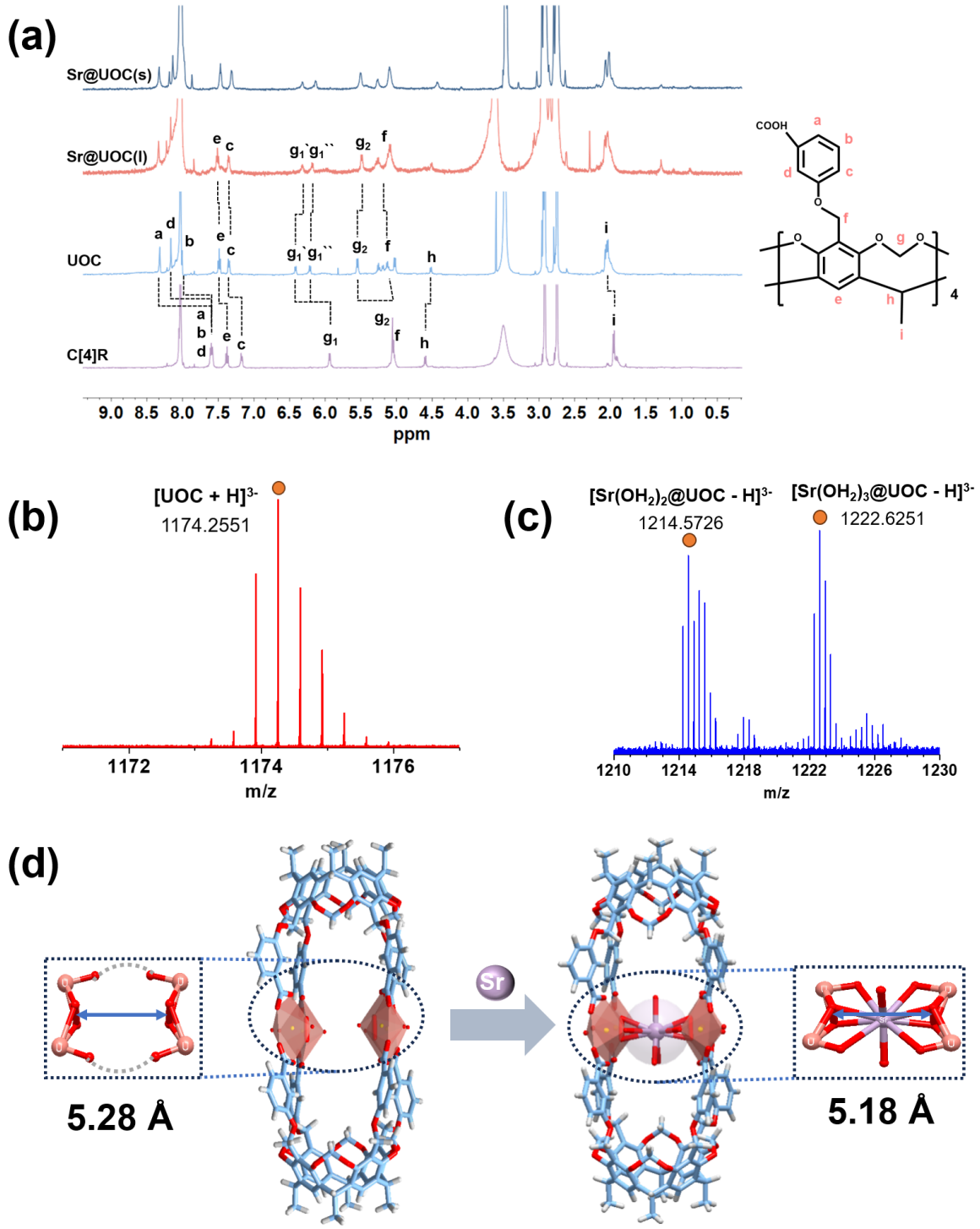

Figure 3. Characterization and comparison of **UOC** and Sr^{2+}-encapsulated **UOC** (Sr@**UOC**): (a) ^{1}H-NMR spectra of C[4]R, **UOC**, and Sr@**UOC** (DMF-d_7, 298 K); (b) high-resolution FT-MS spectra of **UOC** (c) and Sr@**UOC**; (d) a comparison in crystal structure of **UOC** and Sr@**UOC** with a dimension change of the metal-binding pocket before and after Sr^{2+} ion encapsulation.

The diffusion-ordered spectroscopy (DOSY) NMR spectroscopy confirms that, the ^{1}H peaks assigned to **UOC** exhibit identical diffusion rates, indicating the formation of a single discrete structure with a diffusion coefficient of 6.31×10^{-10} $m^2\cdot s^{-1}$ in the solution of DMF-d_7 (**Figure**

S13a), which is ca.2.6 times that of single macrocyclic ligand C[4]R (**Figure S3**). Similarly, the DOSY spectrum of Sr^{2+}-loaded **UOC** also indicates the formation of a new single product, with a diffusion coefficient in DMF-d_7 of 7.41×10^{-10} $m^2\cdot s^{-1}$ (**Figure S13b**). The disparity in diffusion coefficients as revealed by DOSY, together with ^{1}H-NMR, suggest the remarkable interaction of Sr^{2+} ions with **UOC,** and even possible Sr^{2+} encapsulation by **UOC**. Further evidence for the successful encapsulation of Sr^{2+} ions is provided by FT-MS analysis of Sr^{2+}-loaded **UOC** that is isolated after being soaked in a 0.5 M aqueous solution of Sr^{2+} ions for 12 hours. In contrast to the signal of Sr-free UOC (**Figure 3b**), triply charged negative ion peaks at m/z = 1214.5726 and m/z = 1222.6251 corresponding to the chemical compositions $[C_{136}H_{103}O_{52}U_4Sr(OH_2)_2]^{3-}$ and $[C_{136}H_{103}O_{52}U_4Sr(OH_2)_3]^{3-}$, respectively, can be observed (**Figure 3c** and **Figure S14**). These characteristic peaks are attributed to the inclusion of strontium ion in **UOC** together with additional two or three water molecules that coordinate to strontium to form metal complexes with favorable saturated coordination numbers.

The encapsulation of Sr^{2+} by **UOC** is further demonstrated by single crystal structure analysis of Sr-loaded **UOC** (namely Sr@**UOC, Figure 3d**), which helps to unveil the molecular mechanism of Sr^{2+} encapsulation. As revealed by the crystal structure of Sr@**UOC**, a single Sr^{2+} ion is encapsulated within the cryptand-like pocket of **UOC**, situated in a tricapped trigonal prismatic coordination sphere (each peroxo is taken as a distorted capped vertex, **Figure S16**), which is eleven-fold coordinated by four peroxide oxygen atoms, four uranyl axial oxygen atoms, and three aquo oxygen donors, with Sr-O distances ranging from 2.55(7) to 3.21(2) Å (**Table S3**). The restricted flexibility of side chains of C[4]R, coupled with the constraints of its rigid skeleton, allow the unclosed cryptand-like cavity to have a high degree of coordination flexibility within a certain spatial range to accommodate the coordination needs of strontium ions. Specifically, upon coordination with Sr^{2+} at the central site, the minimum diameter of the cryptand-like cavity is adaptably contracted from 5.28 Å to 5.18 Å (**Figure 3d**), and the geometric conformation of flexible arms at each end relative to the uranium center tends to be uniform after Sr binding, improving the overall symmetry of the capsule. This corresponds to the observed reduction in splitting of the side chain methylene in NMR

discussed above. Analysis of the PXRD patterns of the encapsulated powder samples indicated recognizable changes in diffraction peak positions after loading with Sr^{2+} (**Figure S17**). This shift is attributed to strontium adsorption at the internal cryptand-like binding site in Sr@**UOC**, occupying the central positions within the cavity, resulting in a minor structural transformation and subsequent crystal packing compared to the pristine **UOC** (**Figure S18**).

The precise size-matching effect enables the incorporation of Sr^{2+} into specially arranged internal oxygen binding sites in **UOC** to form endo-spherical complexes with high coordination numbers up to 11. Density functional theory (DFT) calculation shows there is overlapping between Sr 4d and O 2p orbitals, conferring the origin of high binding strength of UOC for Sr^{2+} (**Figure 4a**). Besides size-matching effects and the synergistic action of metal coordination bonds, electrostatic potential (ESP) diagram (**Figure S19b**) indicated that host-guest binding is also driven by Coulomb interactions, with the charge of the anionic capsule being compensated by the entry of Sr^{2+}. This conclusion is further supported by the result of the energy decomposition analysis (EDA) analysis, which indicates that electrostatic interaction (Coulomb interactions) predominates in host-guest interactions including partial orbital interaction and very few dispersion interaction (**Figure 4b**).

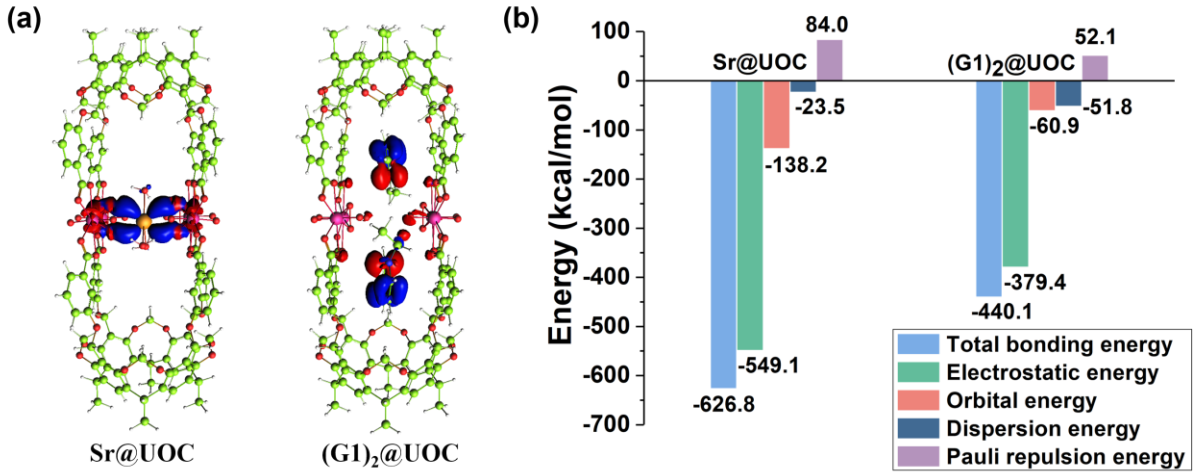

Figure 4. Orbital interaction (a) and EDA calculation (b) of two host-guest complexes of UOC with Sr^{2+} Ion and organic guest 1-ethylpyridinium cation (G1), Sr@**UOC** and $(G1)_2$@**UOC**.

Organic Guest Recognition and Co-encapsulation of Sr^{2+} Ion and Organic Species

Molecular recognition, as a key concept in host-guest chemistry, has significantly advanced the development of coordination cages for guest encapsulation,[14, 60-62] but the challenge of encapsulating different kinds of guest species persists due to the necessity for multiple, specific guest binding sites within a single host structure.[18] Herein, the intriguing multiple-site feature of **UOC** within its capsule cavity, one cryptand-like metal ion site in the middle and two interior hydrophobic sites at both ends, offers distinct binding environments for possible simultaneous encapsulation of both metal ions and organic guests. Therefore, we evaluated further the potential of **UOC** for supramolecular encapsulation of organic guests.

The recognition of organic guests by **UOC** in solution was firstly explored through ^{1}H NMR spectroscopy. Given the cavity's size and total charge distribution (**Figure S19a**), a relatively small, positively charged nitrogen heterocyclic compound, 1-ethylpyridinium bromide (namely as [G1]Br), was selected as a representative guest molecule. In the presence of **UOC**, the spectrum of $[G1]^+$ exhibits noticeable upfield shifts in the proton signals (H_j, H_m, H_n), indicative of significant chemical environment changes when compared to the spectrum of G1 in its free state. These evidences indicate that $[G1]^+$ is encapsulated within the cavity of **UOC** and undergoes a shielding effect as a result of encapsulation. Furthermore, the complexation kinetics results in broadening effects on the proton H_n signals of $[G1]^+$, while the methylene protons of **UOC** experience downfield shifts (**Figure 5a**). Additionally, as demonstrated by the 2D ROESY spectra, the interaction between **UOC** and $[G1]^+$ provides further evidence for encapsulation, with distinct cross-peaks observed between the protons (H_j, H_m) of $[G1]^+$ and **UOC**'s methylene protons (H_g), along with the inward-facing protons (H_d) of the side-chain phenyl rings (**Figure 5b**). The FT-MS analysis shows a set of main peaks centered at m/z = 1868.9608 that are assignable to $[(G1)_2@UOC]^{2-}$ species, thus confirming the $(G1)_2$@**UOC** composition with a molecular weight of 3737.92 Da (**Figure 5c** and **Figure S20**). This speculation is further supported by fluorescence titration analysis (**Figure 5d**), which demonstrates a progressive weakening of fluorescence emission of $[G1]^+$ with the addition of **UOC**.

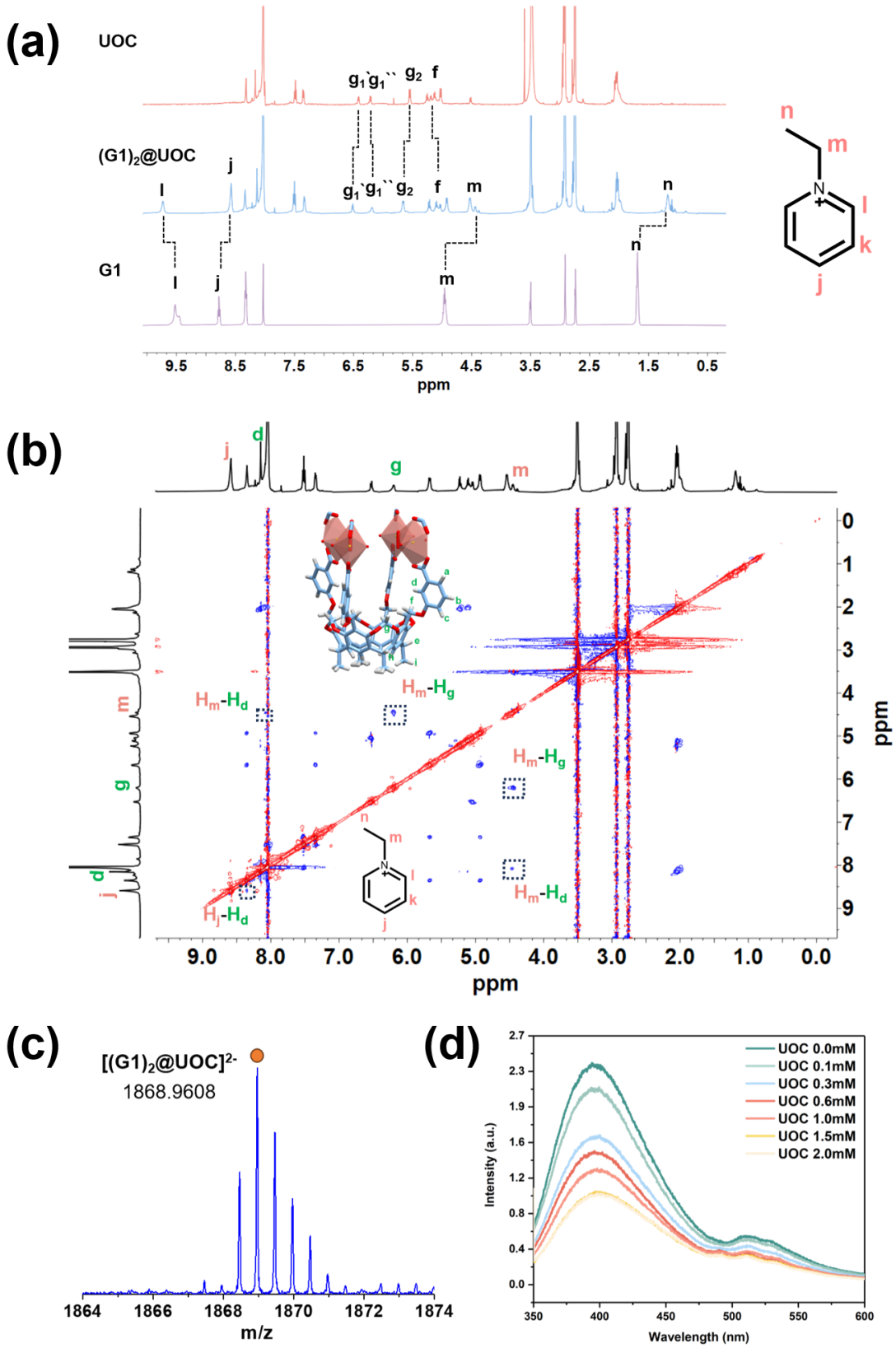

Figure 5. Encapsulation of organic guest species $[G1]^+$ in the cavity of **UOC**: (a) ^{1}H NMR spectra of $[G1]^+$, **UOC**, and $(G1)_2$@UOC (DMF-d_7, 298 K); (b) 2D ROESY spectra of $(G1)_2$@**UOC** (DMF-d_7, 298 K); (c) High-resolution FT-MS spectra of $(G1)_2$@**UOC**; (d) The changes in fluorescence intensity of $[G1]^+$ (4.0 mM, λ_{ex} = 315 nm) upon gradual addition of **UOC** in DMF.

Structural elucidation carried out through single-crystal analysis further unveiled the molecular encapsulation mechanism, revealing that $[G1]^+$ is positioned between two closely spaced side-chain phenyl rings of the **UOC** skeleton, with an average distance of approximately 3.8 Å (**Figure S21**). The distance between the inward-facing proton H_d on the side-chain phenyl rings and H_j of $[G1]^+$ was determined to be 3.0 Å, consistent with the cross-peaks observed in the ROESY spectra. These findings indicate that **UOC**'s hydrophobic cavity engages with G1 through aromatic π-π stacking and van der Waals forces (**Figure 4b**).

Following the validation of **UOC**'s selective recognition capabilities for metal ions and organic species, we further investigated the co-encapsulation of these two different kinds of guest species. ^{1}H NMR spectroscopy of **UOC** that is subject to soaking in a mixed aqueous solution of [G1]Br and strontium ions for 12 hours shows significant changes compared to that of Sr@**UOC** or $(G1)_2$@**UOC** with a single kind of guest species (**Figure 6a**), indicating possible co-encapsulation of both species. FT-MS spectrum of UOC after the above treatment affords further evidence to co-encapsulation, where a distinct peak at m/z = 968.23 should be assigned to be the signal of $[(Sr/(G1)_2)@UOC\text{-}4H]^{4-}$ (**Figure 6b**). Titration experiments of **UOC** (treated by aqueous solution of Sr^{2+} and $[G1]^+$ in turn) recorded by ^{1}H NMR illustrate clearly the detailed encapsulation process: (1) Similar to the trend observed in the previous section, with the addition of Sr^{2+}, deshielding effects on **UOC**'s peripheral hydrogen atoms H_e and H_c with shifts of 0.18 and 0.10 ppm respectively, and a shielding effect on methylene H_g up to 0.14 ppm (**Figure 6c**, Parts B and C) are observed, suggesting occupation of the cryptand-like recognition site by the Sr^{2+} ion enhances the cavity's electron density and alters the surrounding electron density distribution. Meanwhile, the change of UOC's side-chain methylene H_f from quartets to doublets after Sr^{2+} addition is consistent with the observation mentioned above when comparing the NMR spectra of Sr@**UOC** and **UOC**. When the ratio of Sr: **UOC** exceeds 1:1, there is no more change in ^{1}H NMR, indicating the formation of 1:1 complex of **UOC a**nd Sr^{2+}, i.e. Sr@**UOC**. (2) With further addition of $[G1]^+$ into the solution of as-formed Sr@**UOC**, an upfield shift of 0.10 ppm for H_i and a downfield shift of 0.10 ppm for methyl H_n in $[G1]^+$ are observed (**Figure 6c**, Parts A and D), indicating the impact of

aromatic stacking near nitrogen on electron distribution similar to the case after Sr^{2+} encapsulation discussed above. This leads to a pronounced shielding effect in the vicinity of nitrogen atoms, whilst regions distant from nitrogen experience deshielding. This trend aligns with observations made during the titration of $[G1]^+$ directly into Sr@**UOC** (**Figure S24**). Although there are difficulties in cultivating crystal samples suitable for single-crystal diffraction analysis were obtained, the optimized structure of $(Sr/(G1)_2)$@**UOC** (**Figure 6d**) that encapsulates simultaneously two different kinds of guests, i.e. metal ions and organic cations, in the cavity of **UOC** is obtained by DFT calculation based on the principle of lowest energy. Notably, different from the encapsulation of heterogeneous organic guests reported previously, this is the first time that the co-encapsulation of two different kinds of guest species, metal ions and organic aromatic cations, has been achieved in a multi-site MOC host. Apparently, given the inherent recognition ability of traditional MOC for organic guest, the introduction of metal acyl nodes in MOC that enables the effective recognition of second metal ions by MOC is crucial to this co-encapsulation strategy, which fulfills the encapsulation requirements of distinct kinds of guests by designing various coordination environments.[63, 64]

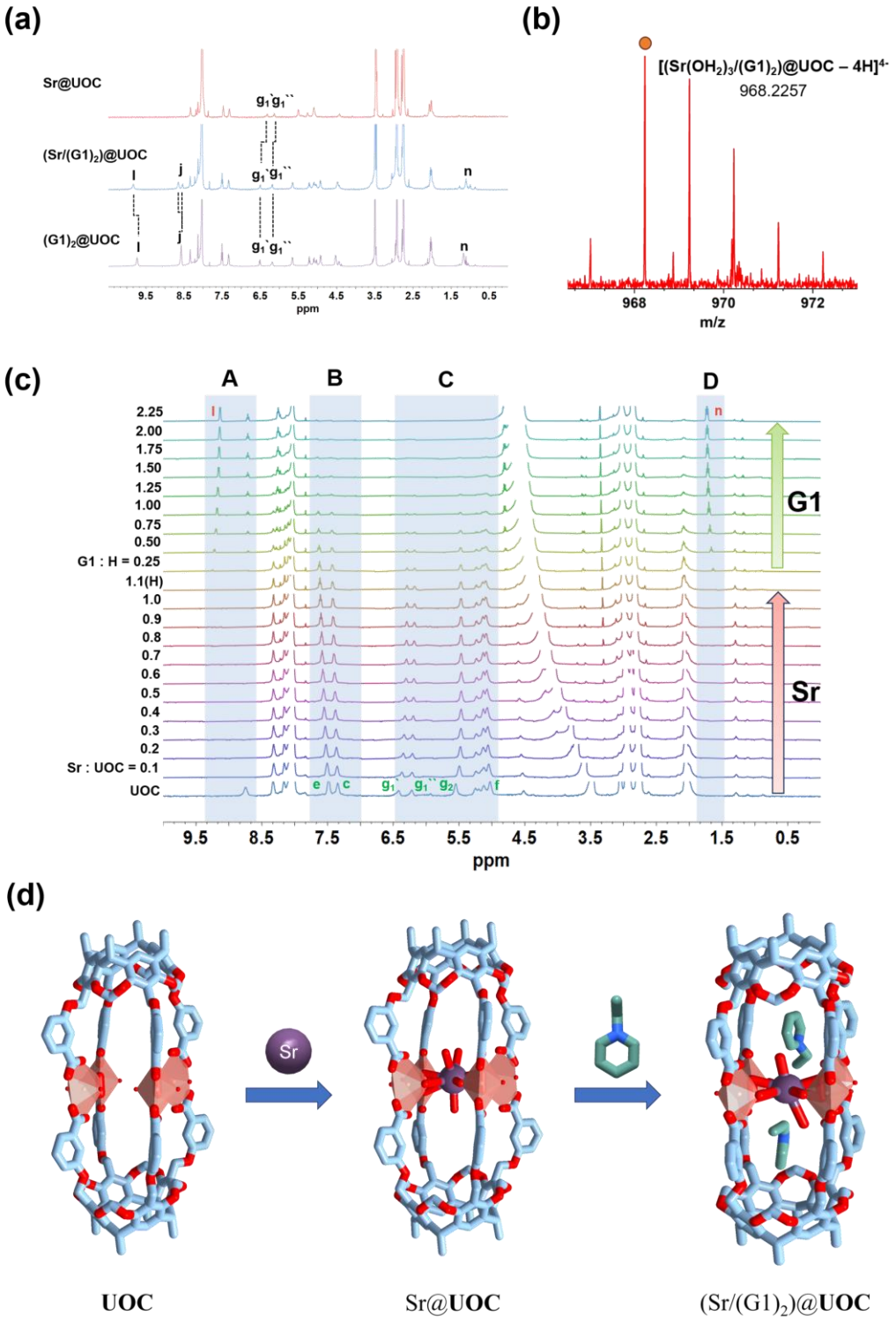

Figure 6. Encapsulation of both Sr^{2+} ions and organic species $[G1]^+$ within the cavity of **UOC**. (a) ^1H NMR spectra of Sr@**UOC**, $(G1)_2$@**UOC**, and $(Sr/(G1)_2)$@**UOC** (DMF-d_7, 298 K). (b) High-resolution FT-MS spectra of $(Sr/(G1)_2)$@**UOC**. (c) ^1H NMR spectra of **UOC** (1.2 mM, DMF-d_7, 298 K) titrated by Sr^{2+} ions and $[G1]^+$(dissolved in D_2O) in turn. From bottom to top, the equivalents of Sr^{2+} ions or $[G1]^+$ gradually increase. (d) The DFT-optimized structure of heterogeneous guest co-encapsulated complex $(Sr/(G1)_2)$@**UOC** with a comparison with crystal structures of **UOC** and Sr@**UOC**.

High-efficiency Removal and Deep Purification of $^{90}Sr^{2+}$ by UOC

The capability of **UOC** to form high-coordination-number inner-sphere complexes with Sr^{2+} ion motivates further investigation into its capacity to remove Sr^{2+} in more competitive contaminated water environments. Prior to the Sr^{2+} adsorption experiments, the chemical stability of **UOC** solid samples were first evaluated. Thermogravimetric analysis (TGA) conducted under a nitrogen atmosphere showed that **UOC** remains stable up to 300 °C, with a slight weight loss observed between 100-250°C due to the dehydration process within the hollow cavity (**Figure S10**). Water stability that is crucial for the application of adsorbents in aqueous environments is also evaluated. The PXRD patterns of solid samples of **UOC** remained unchanged after immersion in water with pH ranging from 3.0 to 10.0 for 24 hours (**Figure S26**). Notably, no leaching of uranyl was detected in the soaking solution when subjected to analysis by inductively coupled plasma optical emission spectroscopy (ICP-OES). These findings suggest that UOC exhibits high water stability across a pH range of 3.0 to 10.0.

Sr^{2+} adsorption performance of **UOC** was investigated by mixing 4 mg of **UOC** with 10 mL of Sr^{2+} solution (10 mg/L, i.e. 10 ppm) at pH 9.0. Adsorption kinetics analysis revealed that Sr^{2+} adsorption by **UOC** reached equilibrium within 6 hours, fitting well with a pseudo-second-order model, indicating Sr^{2+} adsorption to a chemisorption mechanism (**Figure S27**). Isotherm studies on Sr^{2+} adsorption at pH 9, as shown in the **Figure S28**, were well described by the Langmuir model, yielding a maximum adsorption capacity of 23.4 mg/g (0.27 mmol/g) for **UOC**. The calculated maximum adsorption capacity of 24.88 mg/g closely matches the theoretical value based on the inclusion model of 1:1 complex as revealed in Sr@**UOC**. The maximum distribution coefficient (K_d) measured after reaching equilibrium reached to 1.36×10^7 mL/g at the initial Sr^{2+} concentration of 0.35 ppm, which is much larger than that observed in Sr-absorbents based on ion-exchange mechanism[65-67] and is indicative of a strong interaction of **UOC** with Sr^{2+} even at very low concentrations. Consistent with expectations, a removal efficiency of 99.9% could be achieved for Sr^{2+} ions at concentrations as low as 0.01 mM (**Figure 7a**). The excellent removal efficiency at ultra-low Sr^{2+} concentration underscores

the depth of Sr^{2+} decontamination, enabling profound remediation of Sr^{2+} radioisotopes, such as ^{90}Sr, present at trace concentrations.

Given the varied pH levels of contaminated natural water systems, the effect of pH on the adsorption of Sr^{2+} ion by **UOC** was further investigated with pH ranging from 3.0 to 10.0 (**Figure S29**). The results reveal that **UOC** exhibited good Sr^{2+} adsorption capabilities within a wide pH range of 5.0 to 10.0, reaching its highest adsorption capacity at pH 10.0, close to the theoretical maximum adsorption capacity. As shown by zeta potential measurements of **UOC** at various pH levels, an increase in pH leads to an increase in surface charge (**Figure S30**), which might enhance the electrostatic attraction to Sr^{2+} ions, thus improving adsorption capacity with pH rising from 3.0 to 10.0. Specifically, a sharp increase in **UOC**'s surface negative charge is observed as pH increasing from 3.0 to 4.0. When pH is increased to above 5.0, **UOC** exhibits a relatively stable surface negative charge, explaining its consistently strong adsorption capabilities for Sr^{2+} ions within the broad pH range of 5.0-10.0.

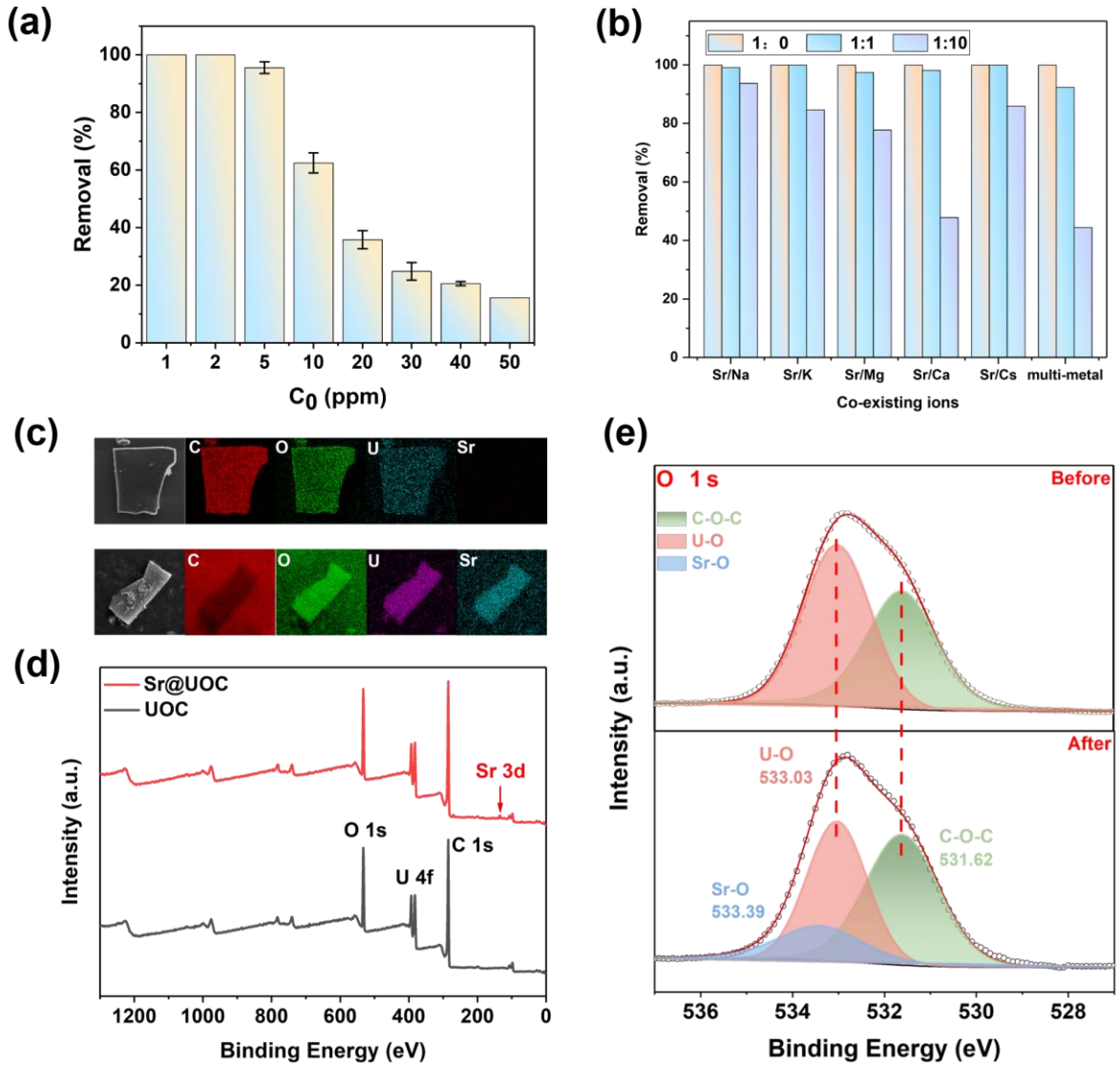

Figure 7. Sr^{2+} ion adsorption and deep purification by **UOC**. (a) Effect of initial Sr^{2+} concentration on Sr^{2+} removal by **UOC**. (b) Influence of coexisting alkali and alkali-earth metal ions on the removal of Sr^{2+} ions. (c) SEM image and EDS mapping of **UOC** before and after Sr^{2+} ion adsorption. (d) XPS spectra of UOC and Sr@UOC. (e) High-resolution O 1s XPS spectra of UOC before and after Sr^{2+} ion adsorption.

Considering the competition of coexisting metal ions to adsorption sites and trace concentrations of Sr^{2+}, we evaluated the interference of Na^{+}, K^{+}, Mg^{2+}, Ca^{2+}, Cs^{+} and a multi-ion mixture of all these five ions on adsorbing 0.01 mM of Sr^{2+} ions in competitive adsorption experiments (**Figure 7b**). The results show that, in the presence of each individual interfering metal ion of equal molar concentration, **UOC**'s removal capacity for Sr^{2+} ion still exceeds 97%, showing no significant drop compared to the nearly perfect removal efficiency without

interfering metal ions. Even when molar concentration of each kind of competitive metal ion is ten times that of Sr^{2+} ion, Sr^{2+} ion removal efficiency remains close to 80%, except for the case of Ca^{2+} as the competitive ion (only 50% removal) which shows high similarity to strontium ions in ionic radius and coordination behavior. A similar removal rate for strontium is achieved in a multi-ion mixture including equal molar concentrations of competitive ions, Na^{+}, K^{+}, Mg^{2+}, Ca^{2+}, Cs^{+}, demonstrating a robust selective binding capability at low ion concentrations. This separation selectivity is in sharp contrast with those adsorbents that remove Sr^{2+} ion based on an ion exchange mechanism through forming outer-sphere complexes[68, 69].

The corresponding elemental mapping analysis of energy dispersive X-ray spectroscopy (EDS) indicates that strontium ions are uniformly distributed within the strontium-loaded UOC, with a U:Sr molar ratio of 4:1 (**Figure 7c**). This is also consistent with that observed in single crystal structure of Sr@**UOC**, demonstrating the efficient utilization of **UOC**'s cryptand-like recognition sites. A comparison of XPS spectra before and after Sr^{2+} ion also confirms the successful adsorption of Sr^{2+} (**Figure 7d** and **Figure S31**). Correspondingly, the binding energy of oxygen atoms in Sr@**UOC** is also different from the pristine sample of **UOC** (**Figure 7e**). This disparity arises from the establishment of a new electronic environment resulting from the interaction between the oxygen atom and the loaded Sr^{2+} ion. a new peak at 533.39 eV emerges, corresponding to the formation of the Sr-O bonds.

CONCLUSION

In summary, we have proposed a method that incorporates peroxo-bridging dimeric uranyl unit as the functional module of MOC for customizing metal ion binding sites within MOC cavities. The as-synthesized uranyl-based MOC, i.e. **UOC**, provides abundant internal cryptand-like binding sites for metal ion anchoring, facilitating inner-sphere recognition of metal ions. Such chelation-based metal binding significantly enhances the recognition ability of **UOC** to Sr^{2+}ion, enabling selective removal and deep purification of trace-level ^{90}Sr across a wide pH range. Furthermore, besides the Sr^{2+}-binding site, there is a second kind of hydrophobic pocket within **UOC**'s cavity, allowing for the co-encapsulation of both metal ion and aromatic organic guests

within a single host structure. This work demonstrates a feasible approach through exquisite structural design to accommodate tailored cavity microenvironments of MOC for efficient recognition of guests. It is believed that, more customized metallo-supramolecular architectures for host-guest recognition of multiple targets will be inspired, thus opening up greater possibilities for the co-recognition, co-transportation, and multimodal catalysis of various kinds of guests that require distinct recognition sites within the same host skeleton.

Acknowledgements

The authors are thankful for support from the National Natural Science Foundation of China (22122609, 22076186 and U20B2019). The National Science Fund for Distinguished Young Scholars (21925603) are also acknowledged.

Keywords: Metal-organic cages • Acyl nodes • Radioactive Strontium • Deep purification • Co-encapsulation

REFERENCES

(1) Pawson, T.; Nash, P., Assembly of cell regulatory systems through protein interaction domains. *Science.* **2003,** *300* (5618), 445-452.

(2) Lunde, B. M.; Moore, C.; Varani, G., RNA-binding proteins: modular design for efficient function. *Nat. Rev. Mol. Cell Biol.* **2007,** *8* (6), 479-90.

(3) Hicke, L.; Schubert, H. L.; Hill, C. P., Ubiquitin-binding domains. *Nat. Rev. Mol. Cell Biol.* **2005,** *6* (8), 610-21.

(4) McConnell, A. J., Metallosupramolecular cages: from design principles and characterisation techniques to applications. *Chem. Soc. Rev.* **2022,** *51* (8), 2957-2971.

(5) Bai, S.; Han, Y. F., Metal-N-Heterocyclic Carbene Chemistry Directed toward Metallosupramolecular Synthesis and Beyond. *Acc. Chem. Res.* **2023,** *56* (10), 1213-1227.

(6) Chakraborty, S.; Newkome, G. R., Terpyridine-based metallosupramolecular constructs: tailored monomers to precise 2D-motifs and 3D-metallocages. *Chem. Soc. Rev.* **2018,** *47* (11), 3991-4016.

(7) Gan, M. M.; Liu, J. Q.; Zhang, L.; Wang, Y. Y.; Hahn, F. E.; Han, Y. F., Preparation and Post-Assembly Modification of Metallosupramolecular Assemblies from Poly(N-Heterocyclic Carbene) Ligands. *Chem. Rev.* **2018,** *118* (19), 9587-9641.

(8) Chakrabarty, R.; Mukherjee, P. S.; Stang, P. J., Supramolecular Coordination: Self-Assembly of Finite Two- and Three-Dimensional Ensembles. *Chem. Rev.* **2011,** *111* (11), 6810-6918.

(9) Smulders, M. M.; Riddell, I. A.; Browne, C.; Nitschke, J. R., Building on architectural principles for three-dimensional metallosupramolecular construction. *Chem. Soc. Rev.* **2013,** *42* (4), 1728-54.

(10) Chen, L. J.; Yang, H. B.; Shionoya, M., Chiral metallosupramolecular architectures. *Chem. Soc. Rev.* **2017,** *46* (9), 2555-2576.

(11) Ronson, T. K.; Zarra, S.; Black, S. P.; Nitschke, J. R., Metal–organic container molecules through subcomponent self-assembly. *Chem. Commun.* **2013,** *49* (25), 2476.

(12) Lee, S.; Jeong, H.; Nam, D.; Lah, M. S.; Choe, W., The rise of metal-organic polyhedra. *Chem. Soc. Rev.* **2021,** *50* (1), 528-555.

(13) Zhang, D.; Ronson, T. K.; Nitschke, J. R., Functional Capsules via Subcomponent Self-Assembly. *Acc. Chem. Res.* **2018,** *51* (10), 2423-2436.

(14) Zhang, D.; Ronson, T. K.; Zou, Y. Q.; Nitschke, J. R., Metal-organic cages for molecular separations. *Nat. Rev. Chem.* **2021,** *5* (3), 168-182.

(15) Ward, M. D.; Hunter, C. A.; Williams, N. H., Coordination Cages Based on Bis(pyrazolylpyridine) Ligands: Structures, Dynamic Behavior, Guest Binding, and Catalysis. *Acc. Chem. Res.* **2018,** *51* (9), 2073-2082.

(16) Custelcean, R., Anion encapsulation and dynamics in self-assembled coordination cages. *Chem. Soc. Rev.* **2014,** *43* (6), 1813-24.

(17) Amouri, H.; Desmarets, C.; Moussa, J., Confined nanospaces in metallocages: guest molecules, weakly encapsulated anions, and catalyst sequestration. *Chem. Rev.* **2012,** *112* (4), 2015-41.

(18) Rizzuto, F. J.; Von Krbek, L. K. S.; Nitschke, J. R., Strategies for binding multiple guests in metal–organic cages. *Nat. Rev. Chem.* **2019,** *3* (4), 204-222.

(19) Zhu, J. L.; Zhang, D.; Ronson, T. K.; Wang, W.; Xu, L.; Yang, H. B.; Nitschke, J. R., A Cavity-Tailored Metal-Organic Cage Entraps Gases Selectively in Solution and the Amorphous Solid State. *Angew. Chem. Int. Ed.* **2021,** *60* (21), 11789-11792.

(20) Zhang, D.; Ronson, T. K.; Lavendomme, R.; Nitschke, J. R., Selective Separation of Polyaromatic Hydrocarbons by Phase Transfer of Coordination Cages. *J. Am. Chem. Soc.* **2019,** *141* (48), 18949-18953.

(21) Zhang, D.; Ronson, T. K.; Mosquera, J.; Martinez, A.; Nitschke, J. R., Selective Anion Extraction and Recovery Using a $Fe^{II}{}_4L_4$ Cage. *Angew. Chem. Int. Ed.* **2018,** *57* (14), 3717-3721.

(22) Vardhan, H.; Yusubov, M.; Verpoort, F., Self-assembled metal–organic polyhedra: An overview of various applications. *Coord. Chem. Rev.* **2016,** *306*, 171-194.

(23) Riddell, I. A.; Smulders, M. M. J.; Clegg, J. K.; Hristova, Y. R.; Breiner, B.; Thoburn, J. D.; Nitschke, J. R., Anion-induced reconstitution of a self-assembling system to express a chloride-binding $Co_{10}L_{15}$ pentagonal prism. *Nat. Chem.* **2012,** *4* (9), 751-756.

(24) Amouri, H.; Mimassi, L.; Rager, M. N.; Mann, B. E.; Guyard-Duhayon, C.; Raehm, L., Host-guest interactions: design strategy and structure of an unusual cobalt cage that encapsulates a tetrafluoroborate anion. *Angew. Chem. Int. Ed.* **2005,** *44* (29), 4543-6.

(25) Desmarets, C.; Poli, F.; Le Goff, X. F.; Muller, K.; Amouri, H., A unique type of a dicobalt cage templated by a weakly coordinated hexafluorophosphate anion: design, structure and solid-state NMR investigations. *Dalton Trans.* **2009,** (47), 10429-32.

(26) Amouri, H.; Desmarets, C.; Bettoschi, A.; Rager, M. N.; Boubekeur, K.; Rabu, P.; Drillon, M., Supramolecular cobalt cages and coordination polymers templated by anion guests: self-assembly, structures, and magnetic properties. *Chem. Eur. J.* **2007,** *13* (19), 5401-7.

(27) Tabuchi, R.; Takezawa, H.; Fujita, M., Selective Confinement of Rare-Earth-Metal Hydrates by a Capped Metallo-Cage under Aqueous Conditions. *Angew. Chem. Int. Ed.* **2022,** *61* (37), e202208866.

(28) Dong, Y.-B. W., P.; Ma, J.-P.; Zhao, X.-X.; Wang, H.-Y.; Tang, B.; Huang, R.-Q., Coordination-Driven Nanosized Lanthanide "Molecular Lantern" with Tunable Luminescent Properties. *J. Am. Chem. Soc.* **2007,** *129* (16), 4872–4873.

(29) Qasem, N. A. A.; Mohammed, R. H.; Lawal, D. U., Removal of heavy metal ions from wastewater: a comprehensive and critical review. *npj Clean Water.* **2021,** *4* (1).

(30) Al-Hazmi, H. E.; Mohammadi, A.; Hejna, A.; Majtacz, J.; Esmaeili, A.; Habibzadeh, S.; Saeb, M. R.; Badawi, M.; Lima, E. C.; Makinia, J., Wastewater reuse in agriculture: Prospects and challenges. *Environ. Res.* **2023,** *236* (Pt 1), 116711.

(31) Mandal, S.; Natarajan, S.; Mani, P.; Pankajakshan, A., Post-Synthetic Modification of Metal-Organic Frameworks Toward Applications. *Adv. Funct. Mater.* **2020,** *31* (4), 2006291.

(32) Li, X.-Z.; Tian, C.-B.; Sun, Q.-F., Coordination-Directed Self-Assembly of Functional Polynuclear Lanthanide Supramolecular Architectures. *Chem. Rev.* **2022,** *122* (6), 6374-6458.

(33) Niu, Z.; Fang, S.; Liu, X.; Ma, J. G.; Ma, S.; Cheng, P., Coordination-Driven Polymerization of Supramolecular Nanocages. *J. Am. Chem. Soc.* **2015,** *137* (47), 14873-6.

(34) He, Y. P.; Yuan, L. B.; Chen, G. H.; Lin, Q. P.; Wang, F.; Zhang, L.; Zhang, J., Water-Soluble and Ultrastable Ti_4L_6 Tetrahedron with Coordination Assembly Function. *J. Am. Chem. Soc.* **2017,** *139* (46), 16845-16851.

(35) Liu, J.; Wang, Z.; Cheng, P.; Zaworotko, M. J.; Chen, Y.; Zhang, Z., Post-synthetic modifications of metal-organic cages. *Nat. Rev. Chem.* **2022,** *6* (5), 339-356.

(36) Nakamura, T.; Kaneko, Y.; Nishibori, E.; Nabeshima, T., Molecular recognition by multiple metal coordination inside wavy-stacked macrocycles. *Nat. Commun.* **2017,** *8* (1), 129.

(37) Sato, H.; Tashiro, K.; Shinmori, H.; Osuka, A.; Murata, Y.; Komatsu, K.; Aida, T., Positive Heterotropic Cooperativity for Selective Guest Binding via Electronic Communications through a Fused Zinc Porphyrin Array. *J. Am. Chem. Soc.* **2005,** *127*, 13086-13087.

(38) Liao, P.; Langloss, B. W.; Johnson, A. M.; Knudsen, E. R.; Tham, F. S.; Julian, R. R.; Hooley, R. J., Two-component control of guest binding in a self-assembled cage molecule. *Chem. Commun.* **2010,** *46* (27), 4932-4.

(39) Loiseau, T.; Mihalcea, I.; Henry, N.; Volkringer, C., The crystal chemistry of uranium carboxylates. *Coord. Chem. Rev.* **2014,** *266-267*, 69-109.

(40) Andrews, M. B.; Cahill, C. L., Uranyl bearing hybrid materials: synthesis, speciation, and solid-state structures. *Chem. Rev.* **2013,** *113* (2), 1121-36.

(41) Mougel, V.; Chatelain, L.; Hermle, J.; Caciuffo, R.; Colineau, E.; Tuna, F.; Magnani, N.; de Geyer, A.; Pecaut, J.; Mazzanti, M., A uranium-based UO_2^+-Mn^{2+} single-chain magnet assembled trough cation-cation interactions. *Angew. Chem. Int. Ed.* **2014,** *53* (3), 819-23.

(42) Sullens, T. A.; Jensen, R. A.; Shvareva, T. Y.; Albrecht-Schmitt, T. E., Cation-Cation Interactions between Uranyl Cations in a Polar Open-Framework Uranyl Periodate. *J. Am. Chem. Soc.* **2004,** *126*, 2676-2677.

(43) Krot, N. N.; Grigoriev, M. S., Cation–cation interaction in crystalline actinide compounds. *Russ. Chem. Rev.* **2004,** *73* (1), 89-100.

(44) Qiu, J.; Burns, P. C., Clusters of actinides with oxide, peroxide, or hydroxide bridges. *Chem. Rev.* **2013,** *113* (2), 1097-120.

(45) Fairley, M.; Felton, D. E.; Sigmon, G. E.; Szymanowski, J. E. S.; Poole, N. A.; Nyman, M.; Burns, P. C.; LaVerne, J. A., Radiation-Induced Solid-State Transformations of Uranyl Peroxides. *Inorg. Chem.* **2022,** *61* (2), 882-889.

(46) Thangavelu, S. G.; Cahill, C. L., Uranyl-Promoted Peroxide Generation: Synthesis and Characterization of Three Uranyl Peroxo $[(UO_2)_2(O_2)]$ Complexes. *Inorg. Chem.* **2015,** *54* (9), 4208-21.

(47) Ridenour, J. A.; Cahill, C. L., Synthesis, structural analysis, and supramolecular assembly of a series of in situ generated uranyl-peroxide complexes with functionalized 2,2′ -bipyridine and varied carboxylic acid ligands. *New J. Chem.* **2018,** *42* (3), 1816-1831.

(48) Doyle, G. A. G., D. M. L.; Sinden, A.; Williams, D. J., Conversion of Atmospheric Dioxygen to a μ–η^2,η^2-Peroxo Bridge in a Dinuclear Uranium (VI) Complex. *Chem. Commun.* **1993**, 1170-1172.

(49) Lee, J.; Brewster, J. T.; Song, B.; Lynch, V. M.; Hwang, I.; Li, X.; Sessler, J. L., Uranyl dication mediated photoswitching of a calix[4]pyrrole-based metal coordination cage. *Chem. Commun.* **2018,** *54* (68), 9422-9425.

(50) Mei, L.; Wu, Q. Y.; Wu, S.; Geng, J. S.; Liu, Y. L.; Hu, K. Q.; Liu, Y. C.; Zhang, Z. H.; Liang, Y. Y.; Chai, Z. F.; Burns, P. C.; Shi, W. Q., High-Temperature Synthesis of a Uranyl Peroxo Complex Facilitated by Hydrothermally In Situ Formed Organic Peroxide. *Inorg. Chem.* **2021,** *60* (4), 2133-2137.

(51) Qiu, J.; Vlaisavljevich, B.; Jouffret, L.; Nguyen, K.; Szymanowski, J. E.; Gagliardi, L.; Burns, P. C., Cation templating and electronic structure effects in uranyl cage clusters probed by the isolation of peroxide-bridged uranyl dimers. *Inorg. Chem.* **2015,** *54* (9), 4445-55.

(52) Feng, L.; Chen, X.; Cao, M.; Zhao, S.; Wang, H.; Chen, D.; Ma, Y.; Liu, T.; Wang, N.; Yuan, Y., Decorating Channel Walls in Metal-Organic Frameworks with Crown Ethers for Efficient and Selective Separation of Radioactive Strontium(II). *Angew. Chem. Int. Ed.* **2023,** *62* (45), e202312894.

(53) Wu, L.; Wang, H.; Kong, X.; Wei, H.; Chen, S.; Chi, L., High strontium adsorption performance of layered zirconium phosphate intercalated with a crown ether. *RSC Adv.* **2023,** *13* (10), 6346-6355.

(54) An, S.; Xu, Q.; Ni, Z.; Hu, J.; Peng, C.; Zhai, L.; Guo, Y.; Liu, H., Construction of Covalent Organic Frameworks with Crown Ether Struts. *Angew. Chem. Int. Ed.* **2021,** *60* (18), 9959-9963.

(55) Andrews, C. G.; Macdonald, C. L. B., Crown Ether Ligation: An Approach to Low‐Oxidation‐State Indium Compounds. *Angew. Chem. Int. Ed.* **2005,** *117* (45), 7619-7622.

(56) Cooper, B. F. T.; Andrews, C. G.; Macdonald, C. L. B., The insertion reactions of "crowned" indium(I) trifluoromethanesulfonate into carbon-chlorine bonds. *J. Org. Chem.* **2007,** *692* (13), 2843-2848.

(57) Cooper, B. F. T.; Macdonald, C. L. B., Synthesis and structure of an indium(I) "crown sandwich". *J. Org. Chem.* **2008,** *693* (8-9), 1707-1711.

(58) Wang, Y.; Hu, S.-X.; Cheng, L.; Liang, C.; Yin, X.; Zhang, H.; Li, A.; Sheng, D.; Diwu, J.; Wang, X.; Li, J.; Chai, Z.; Wang, S., Stabilization of Plutonium(V) Within a Crown Ether Inclusion Complex. *CCS Chem.* **2020,** *2* (4), 425-431.

(59) Kusukawa, T.; Yoshizawa, M.; Fujita, M., Probing Guest Geometry and Dynamics through Host-Guest Interactions. *Angew. Chem. Int. Ed.* **2001,** *40* (10), 1879-1884.

(60) Ariga, K.; Ito, H.; Hill, J. P.; Tsukube, H., Molecular recognition: from solution science to nano/materials technology. *Chem. Soc. Rev.* **2012,** *41* (17), 5800-35.

(61) Dong, J.; Davis, A. P., Molecular Recognition Mediated by Hydrogen Bonding in Aqueous Media. *Angew. Chem. Int. Ed.* **2021,** *60* (15), 8035-8048.

(62) Escobar, L.; Ballester, P., Molecular Recognition in Water Using Macrocyclic Synthetic Receptors. *Chem. Rev.* **2021,** *121* (4), 2445-2514.

(63) Preston, D.; Lewis, J. E.; Crowley, J. D., Multicavity $[Pd_nL_4]^{2n+}$ Cages with Controlled Segregated Binding of Different Guests. *J. Am. Chem. Soc.* **2017,** *139* (6), 2379-2386.

(64) Yazaki, K.; Akita, M.; Prusty, S.; Chand, D. K.; Kikuchi, T.; Sato, H.; Yoshizawa, M., Polyaromatic molecular peanuts. *Nat. Commun.* **2017,** *8*, 15914.

(65) Guo, Y.-L.; Sun, H.-Y.; Zeng, X.; Lv, T.-T.; Yao, Y.-X.; Zhuang, T.-H.; Feng, M.-L.; Huang, X.-Y., Efficient removal of Sr^{2+} ions by a one-dimensional potassium phosphatoantimonate. *Chem. Eng. J.* **2023,** *460*.

(66) Feng, M. L.; Sarma, D.; Gao, Y. J.; Qi, X. H.; Li, W. A.; Huang, X. Y.; Kanatzidis, M. G., Efficient Removal of $[UO_2]^{2+}$, Cs^{+}, and Sr^{2+} Ions by Radiation-Resistant Gallium Thioantimonates. *J. Am. Chem. Soc.* **2018,** *140* (35), 11133-11140.

(67) Zhang, J.; Chen, L.; Dai, X.; Zhu, L.; Xiao, C.; Xu, L.; Zhang, Z.; Alekseev, E. V.; Wang, Y.; Zhang, C.; Zhang, H.; Wang, Y.; Diwu, J.; Chai, Z.; Wang, S., Distinctive Two-Step Intercalation of Sr^{2+} into a Coordination Polymer with Record High ^{90}Sr Uptake Capabilities. *Chem.* **2019,** *5* (4), 977-994.

(68) Dyer, A.; Chimedtsogzol, A.; Campbell, L.; Williams, C., Uptake of caesium and strontium radioisotopes by natural zeolites from Mongolia. *Micropor. Mesopor. Mat.* **2006,** *95* (1-3), 172-175.

(69) Fuller, A. J.; Shaw, S.; Peacock, C. L.; Trivedi, D.; Burke, I. T., EXAFS Study of Sr sorption to Illite, Goethite, Chlorite, and Mixed Sediment under Hyperalkaline Conditions. *Langmuir.* **2016,** *32* (12), 2937-46.

Graphical Abstract:

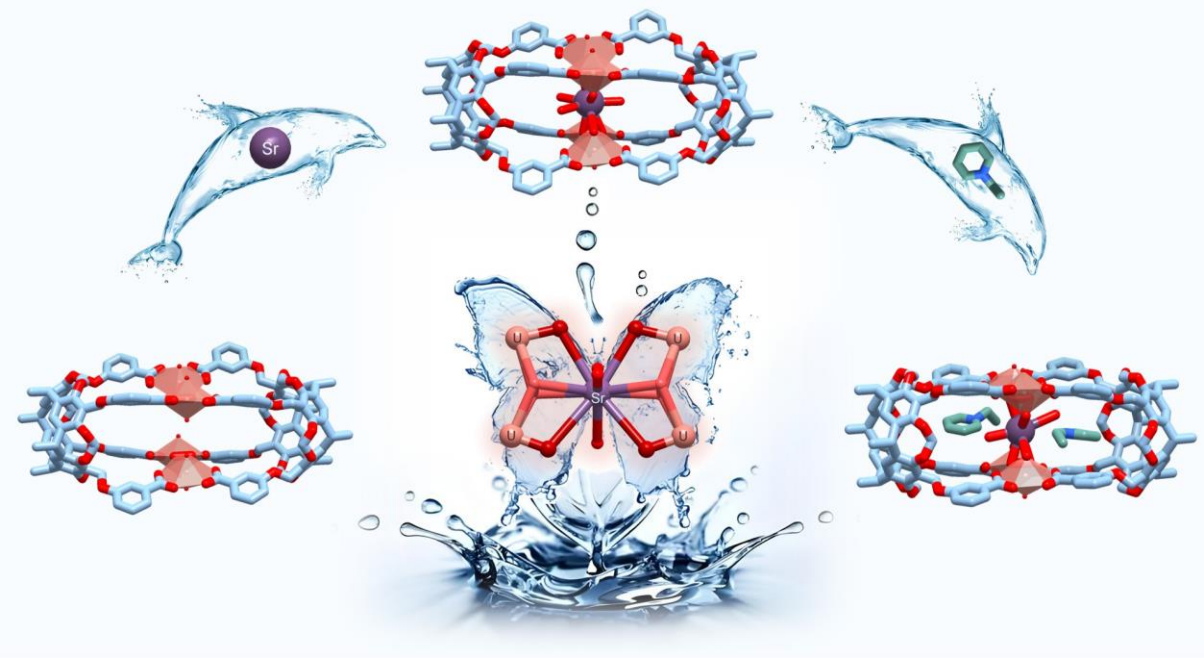

Engineering metal-organic cages (MOCs) with metal acyl nodes leverages axial oxygen atoms of acyl nodes as complementary internal binding groups for supramolecular recognition of metal ions. The resultant uranyl-based MOC (**UOC**) enables efficient encapsulation of Sr^{2+} within the cryptand-like cavity by metal-ligand coordination, facilitating selective removal and deep purification of trace-level Sr^{2+}. Additionally, the other kind of hydrophobic cavities at both ends of the coordination cage in **UOC** allow for recognition of organic guests and facilitate multiple guest co-recognition.